The Central Kiloparsec of Starbursts and AGN: The La Palma Connection
ASP Conference Series, Vol. 000, 2001
J. H. Knapen, J. E. Beckman, I. Shlosman, and T. J. Mahoney, eds.

X-ray Properties of the Central kpc of AGN and Starbursts: The Latest News from Chandra

Kimberly A. Weaver

Code 662, NASA/GSFC, Greenbelt MD 20771 USA
Department of Physics & Astronomy, Bloomberg Center, Johns Hopkins University, Baltimore, MD 21218, USA

Abstract. The X-ray properties of 15 nearby ($v < 3,000$ km s^{-1}) galaxies that possess AGN and/or starbursts are discussed. Two-thirds have nuclear extended emission on scales from ~ 0.5 to ~ 1.5 kpc that is either clearly associated with a nuclear outflow or morphologically resembles an outflow. Galaxies that are AGN-dominated tend to have linear structures while starburst-dominated galaxies tend to have plume-like structures. Significant X-ray absorption is present in the starburst regions, indicating that a circumnuclear starburst is sufficient to block an AGN at optical wavelengths. Galaxies with starburst activity possess more X-ray point sources within their central kpc than non-starbursts. Many of these sources are more luminous than typical X-ray binaries. The *Chandra* results are discussed in terms of the starburst-AGN connection, a revised unified model for AGN, and possible evolutionary scenarios.

1. Introduction

Approximately 20% of local galaxies possess some form of nuclear activity. Such activity ranges from the release of gravitational energy from accretion onto a supermassive ($\sim 10^6 - 10^8$ M$_\odot$) black hole to the cumulative effects of short-lived episodes of star formation. Active galactic nuclei (AGN) and starburst activity often co-exist, but because of their different observational properties, they have historically been studied as independent phenomena.

There are many pieces to the nuclear-activity puzzle. X-rays that are emitted near a supermassive black hole, whether from the base of a jet, from the accretion disk corona or by some other mechanism, are an excellent means of probing the matter within a few to tens of gravitational radii ($r_{\rm g}$=GM/c^2) via absorption, scattering or fluorescence in the accreting material. On larger scales, X-rays probe star-forming regions, starburst-driven nuclear outflows and AGN-driven outflows. On their journey out of the galaxy core, X-rays are absorbed and/or interact in other ways with surrounding material (torus, molecular clouds) to produce regions such as photoionized "warm" absorbers and hot electron scattering "mirrors".

There is also a new class of X-ray emitting objects: the so-called ultra-luminous compact X-ray sources (ULXs, Makishima et al. 2000) or intermediate-luminosity X-ray sources (IXOs). These objects have 0.1–2.4 keV luminosities higher than the Eddington luminosity of a 1.4 solar mass accreting neutron

star ($L_X > 10^{38}$ erg s^{-1}). About half of normal galaxies contain such sources (Colbert & Mushotsky 1999). Their nature is unclear but these compact objects may be accreting "middleweight" black holes with masses on the order of 100 to 1,000 $M_\odot$ (Makishima et al. 2000) or stellar-mass black holes that are beamed toward us or emit anisotropically (King et al. 2001).

To understand the connection between starbursts and AGN it is important to learn how these two phenomena influence their common environment. For example, the onset of a central starburst correlates with a higher probability of obscuring the AGN broad line region (Maiolino et al. 1995). This suggests that the presence or absence of a starburst is sometimes responsible for how we choose to classify an AGN. Progress in this area of study requires the ability to disentangle the emission processes of circumnuclear starbursts from AGN, observations that are now possible in the X-ray band with *Chandra*.

2. The data

The X-ray data discussed here were obtained with the ACIS-S experiment on-board the *Chandra* X-ray observatory. All but three data sets are currently in the public archive. If published, results from the literature are reviewed. Table 1 lists the galaxies, their NED classification and a secondary classification (if available) in parenthesis.

Table 1. *Chandra* Observations of Nearby Starbursts and AGN

Galaxy	Type[(1)]	z[(2)]	D[(3)] (Mpc)	Scale[(3)] (pc/″)	ObsID[(4)]	Time[(5)] (ks)
NGC 253	Stb	0.0008	3	13	969	15.0
NGC 1068	S2 (Stb)	0.0038	23	110	344	50.0
NGC 2110	S2	0.0078	47	210	883	50.0
MCG−5-23-16	S1.9	0.0083	50	240	2121	80.0
M 82	Stb	0.0007	4	19	361	34.0
NGC 3079	S2/L (Stb)	0.0038	23	110	2038	30.0
NGC 3256	Merger(Stb)	0.0091	55	270	835	25.0
NGC 3628	L (Stb)	0.0028	16	70	2039	60.0
NGC 4051	S1.5	0.0024	14	60	859	80.0
NGC 4151	S1.5	0.0033	20	90	348	30.0
NGC 4258	S1.9/L	0.0015	9	44	350	14.5
NGC 4579	S1.9/L	0.0051	30	140	807	35.0
NGC 4945	S2 (Stb)	0.0019	11	53	864	50.0
M 51	S2	0.0015	8	40	354	15.0
Circinus	S2 (Stb)	0.0015	4	19	356	25.0

Notes.—(1) NED classification. Symbols are: S1.5, 1.9, 2 = Seyfert classification, Stb = starburst, L = LINER. Parenthesis list additional classification. (2) Redshifts are from NED. (3) Distances are calculated assuming $H_0 = 50$ km s^{-1} Mpc^{-1}. (4) *Chandra* observation ID. (5) Archived exposure time.

At the time of this writing, the ACIS spectral calibration was being revised (http://asc.harvard.edu/). I therefore focus primarily on imaging results.

3. AGN and AGN-Powered X-rays

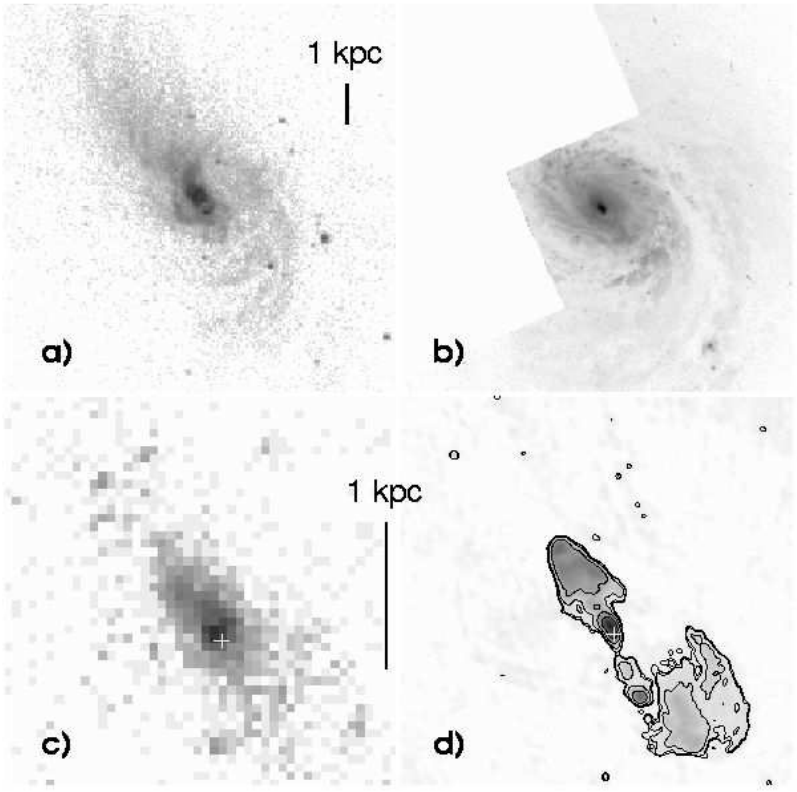

Figure 1. Images of NGC 1068. *a)* Raw, unbinned 0.2–8.5 keV *Chandra* image. Pixels are $0.5'' \times 0.5''$; image size is $1.5' \times 1.5'$ (9.9 kpc × 9.9 kpc). *b)* *HST* WFPC image plotted on the same scale. *c)* Enlargement of the central $22'' \times 22''$ (2.4 kpc × 2.4 kpc) region in hard X-rays (2.5–8.5 keV). *d)* VLA 6 cm radio map (Wilson & Ulvestad 1983) plotted on the same scale. *Crosses* mark the position of the radio nucleus.

3.1. NGC 1068

NGC 1068 is a Seyfert 2 galaxy harboring an intense starburst ring within its central ~ 2 kpc. X-ray emission covers much of the inner region of the galaxy (Fig. 1*a*) and shows a wispy structure similar to the spiral arms (Fig. 1*b*). Figure 1*c* shows an enlargement of the central region. A bright compact X-ray source extends $\sim 1.5''$ (165 pc) in the direction of the nuclear radio continuum emission (Young, Wilson & Shopbell 2001). Bright X-ray emission also extends $5''$ (550 pc) to the NE coinciding with the northeast radio lobe (Fig. 1*d*) and high-excitation ionized gas seen in [O III] λ5007 images.

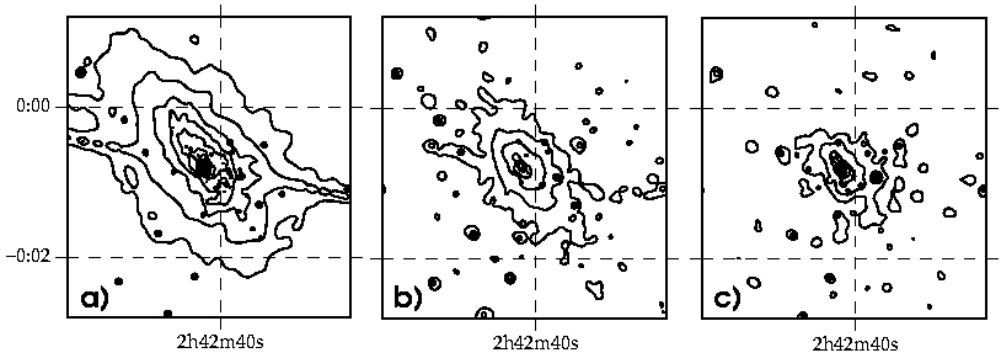

Figure 2. Contours for adaptively smoothed images of NGC 1068 for energy bands *a)* 0.2–1.5 keV, *b)* 1.5–2.5 keV and *c)* 2.5–8.5 keV. Image size is $4' \times 4'$ (26.4 kpc × 26.4 kpc for $H_0 = 50$ km s^{-1} Mpc^{-1}).

The X-ray morphology in different energy bands offers a clue as to whether the X-ray emission is associated with the AGN or the starburst. Young, et al. (2001) argue that the starburst contributes little to the X-rays because the large-scale emissions are fairly well aligned and they do not correlate with the $\sim$ 2 kpc starburst ring. Figure 2 shows that this is clearly the case for the soft and medium X-ray bands, while the outer contours of the hard X-ray map are slightly less elliptical. Hard X-ray emission extends up to 2.2 kpc from the nucleus, including Fe K emission.

Using the ACIS-S data, Young, Wilson & Shopbell (2001) rule out models consisting of hot plasma emission because such models yield implausibly low abundances. Instead they claim that the large-scale X-ray emission arises from photoionization and fluorescence of the gas by radiation from the Seyfert nucleus. With a complimentary *Chandra* grating observation, Ogle (2001) finds that the nuclear spectrum also contains H-like and He-like resonance lines that are stronger than expected for pure recombination and probably due to resonance scattering. The off-nuclear spectrum also contains strong resonance lines due either to resonance scattering or thermal emission. So a contribution from the starburst cannot be ruled out.

3.2. NGC 2110

The *Chandra* image of NGC 2110 is shown in Figure 3. Soft X-ray emission extends $\sim 40''$ ($\sim$8.4 kpc) in the direction of the galaxy major axis. At the nucleus, soft X-ray emission extends on the order of $5''$(1 kpc) along the direction of the highest excitation optical emission line gas and the 6-cm radio jet (Fig. 3*c*). There are enough counts from the region surrounding the radio/X-ray jet to obtain a crude spectrum. The spectrum can be modeled with a Mekal plasma with kT$\sim$ 0.6 keV and 0.05 Z$_\odot$ or a power law with $\Gamma \sim 4$. The requirement for unphysically low abundances is similar to the result for NGC 1068 (§3.1).

Emission above 2 keV is spatially unresolved. The core is absorbed with $N_{\rm H} = 3 \times 10^{22}$ cm^{-2} and an X-ray flux of 3×10^{-11} erg cm^{-2} s^{-1}. About $^3/_4$ of

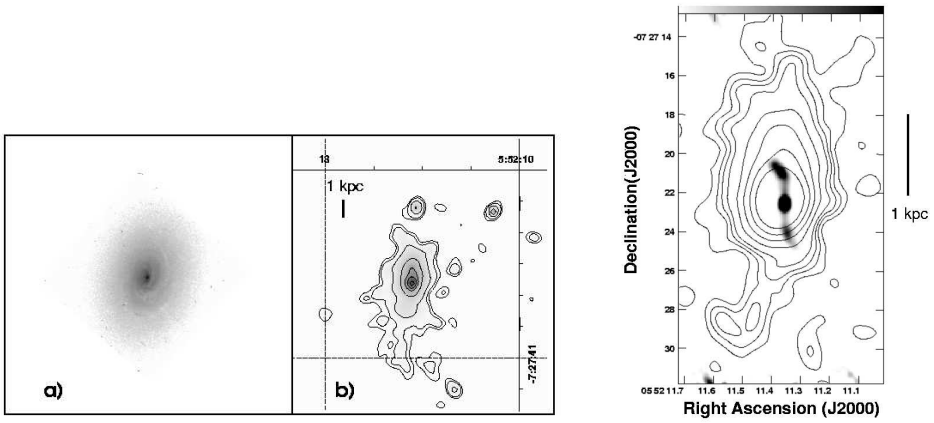

Figure 3. *a) HST* WFPC *image* of NGC 2110 compared with *b)* the soft X-ray *Chandra* contours (0.2–1.5 keV). The image sizes are $60'' \times 63''$ and the X-ray image in *b)* is smoothed to a resolution of $2''$. *c)* Enlargement of the central region showing the nuclear soft X-ray *contours* overlaid on the 6 cm radio map (Ulvestad & Wilson 1983).

the soft X-ray emission at the nucleus can be described as the result of partial covering of the continuum source while about $^1/_4$ is consistent with thermal emission with a temperature of 0.6 keV and solar abundances.

3.3. MCG−5-23-16

The importance of the Fe Kα line for studying the accretion phenomenon in AGN was solidified by *ASCA*, which discovered extremely broad and asymmetric lines (Nandra et al. 1997). Observations of MCG−5-23-16 with *ASCA* suggested that the Fe Kα line has a narrow core and a broad component (Weaver et al. 1997).

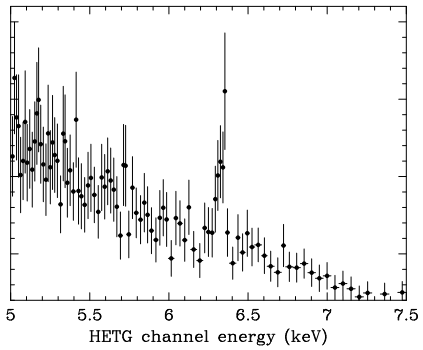

Figure 4. HETG spectrum of the Fe Kα line in MCG−5-23-16.

The *Chandra* HETG spectrum of MCG−5-23-16 is shown in Figure 4. The 6.4 keV line is narrow with FWHM $< 3,000$ km s^{-1} and an equivalent width of $\sim$ 90 eV (about $^1/_2$ the *ASCA* EW). The *ASCA* broad component is not

detectable in the *Chandra* spectrum. Modeling the line as emission from a geometrically thin accretion disk yields a lower limit to the line-emitting region of 200 $r_{\rm g}$ (units of GM/c^2).

3.4. NGC 3079

Figure 5 shows a false-color ACIS-S image of the soft X-ray emission from NGC 3079 (Strickland et al., in prep). The soft X-ray filaments align well with Hα + N II emission from the wind-blown nuclear superbubble, which has a velocity of $\sim 2,000$ km s^{-1} and diameter of 1.1 kpc (Veilleux et al. 1994).

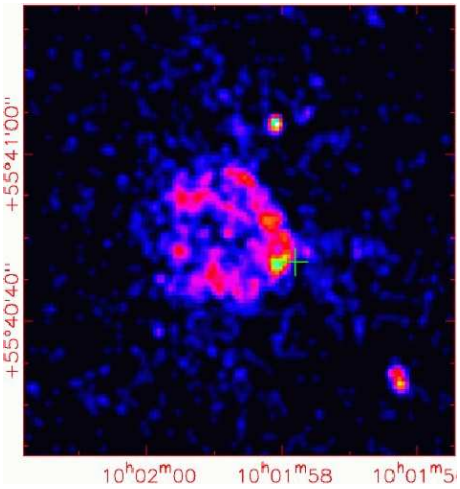

Figure 5. False-color soft X-ray image of NGC 3079. The image is 5 kpc $\times$ 5 kpc, smoothed with a FWHM 1.0″ Gaussian. The green cross shows the position of the nucleus.

3.5. NGC 4051

Figure 6 compares the optical DSS image of NGC 4051 with the zero order *Chandra* HETG soft and hard X-ray images. There is no evidence for extended emission (see also Collinge et al. 2001).

NGC 4051 possesses an ionized absorber with $N_{\rm H} = 10^{20-21}$ cm^{-2}. The *Chandra* spectrum shows emission lines from various hydrogen-like and helium-like ions of O, Ne, Mg and Si as well as blueshifted X-ray absorption systems at -2340 ± 130 km s^{-1} and -600 ± 130 km s^{-1}. The high ratio of forbidden to resonance lines implies that the plasma is photoionized with little collisional ionization (Collinge et al. 2001).

The Fe Kα emission line at 6.4 keV has a FWHM of less than 2,800 km s^{-1} and an EW of 158 eV. This line is significantly narrower than an accretion disk line and, like MCG−5-23-16, indicates emission from farther out in the galaxy core.

Within 1 kpc of the nucleus there is a single X-ray point source, which shows up in the soft image to the SE of the nucleus. It has a 0.5–8 keV X-ray luminosity of $\sim 1.4 \times 10^{38}$ erg s^{-1}, consistent with an X-ray binary accreting at the Eddington limit.

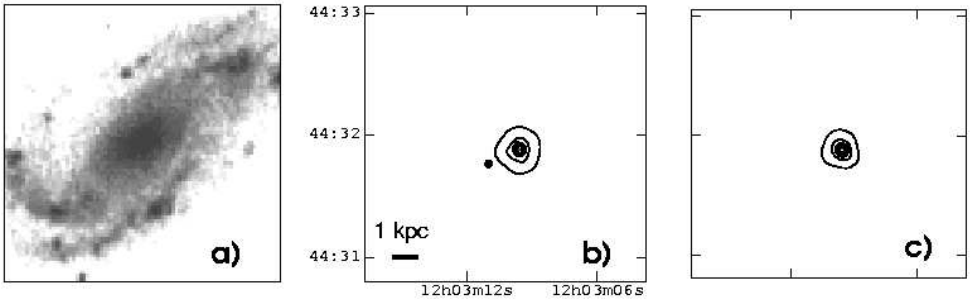

Figure 6. Images of the central $2.4'' \times 2.4''$ (8.5 kpc $\times$ 8.5 kpc) region of NGC 4051. *a)* Optical Digitized Sky Survey image. *b)* Contours for the smoothed *Chandra* HETG zero-order 0.2–1.5 keV image. *c)* Contours for the smoothed 2.5–8.5 keV HETG zero-order image.

3.6. NGC 4151

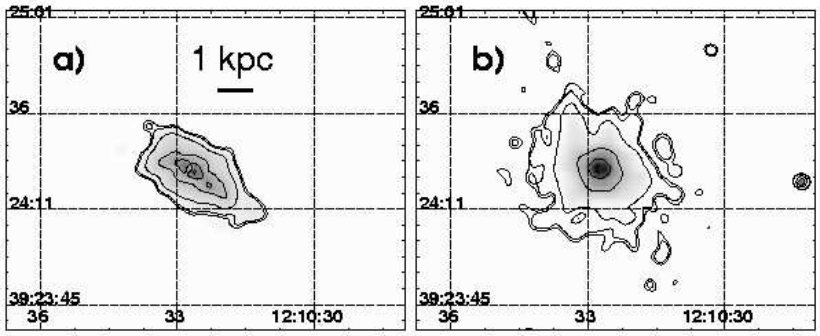

Figure 7. Unbinned and adaptively smoothed greyscale *Chandra* images of NGC 4151 with *contours* overlaid. Image sizes are $1.8' \times 1.4'$ (9.7 kpc $\times$ 7.6 kpc) and are shown for energy bands *a)* 0.2–1.5 keV (soft) and *b)* 2.5–8.5 keV (hard).

About 70% of the soft X-ray emission in NGC 4151 is spatially resolved (Ogle et al. 2000) with an extent of $\sim$ 1.6 kpc SW of the nucleus (Fig. 7*a*), similar to the optical NLR emission. Whether the hard X-rays are extended is unclear. From ACIS-S (non-grating) data, Yang, Wilson & Ferruit (2001) claim that energies > 2 keV are spatially unresolved. However, from grating observations, Ogle et al. (2000) infer that some of the narrow Fe Kα emission comes from the extended NLR.

The *Chandra* grating spectrum is dominated by narrow emission lines. The X-ray NLR is composite, consisting of both photoionized (T = 3×10^4 K) and

collisionally ionized (T = 10^7 K) components, indicating a two-phase medium (Ogle et al. 2000).

3.7. NGC 4258

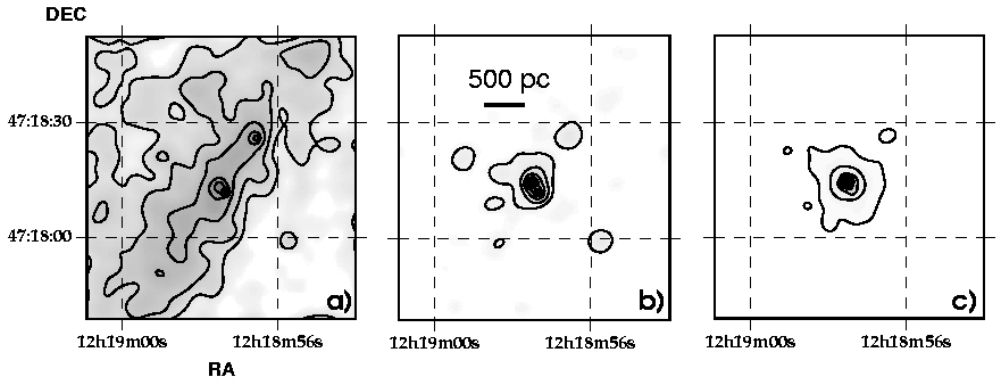

Figure 8. Smoothed greyscale ACIS images of NGC 4258 with *contours* overlaid. Image size is $71'' \times 76''$ (2.5 kpc × 2.6 kpc). Images are divided into *a)* 0.2–1.5 keV, *b)* 1.5–2.5 keV and *c)* 2.5–8.5 keV.

Chandra images of NGC 4258 are shown in Figure 8. The soft X-ray emission is extended and trails along the "anomalous arms" of the galaxy. The large-scale emission and its relation to the radio jets is discussed in detail by Wilson, Yang & Cecil (2001). There is little emission extended at harder energies.

There are two point sources in the core, with the one to the SW being brighter in soft X-rays (Fig. 8*a*). The NE source dominates the hard X-ray image (Fig. 8*c*) and coincides with the radio continuum core of the galaxy and nuclear H_2O maser source (Wilson, et al. 2001). This is the location of the buried AGN. *SAX* observations measure $N_{\rm H} = 9.5 \times 10^{22}$ cm^{-2} (Fiore et al. 2001). The SW source has properties consistent with an XRB.

3.8. NGC 4579

The *Chandra* contours of NGC 4579 are shown in Figure 9, overlaid on an *HST image*. The soft X-ray emission is extended on a scale of ~ 1 kpc on either side of the nucleus. The hard X-rays are confined to the core, presumably from the AGN.

There is a single off-nuclear X-ray point source about $7''$ from the core of the galaxy and possibly a few other faint point sources.

3.9. M 51

Chandra images of M 51 are shown in Figure 10. The 6 cm and 20 cm radio contours correspond well to the extended X-ray emission north and south of the core (Terashima & Wilson 2001). The northern outflow is ~ 800 pc across and

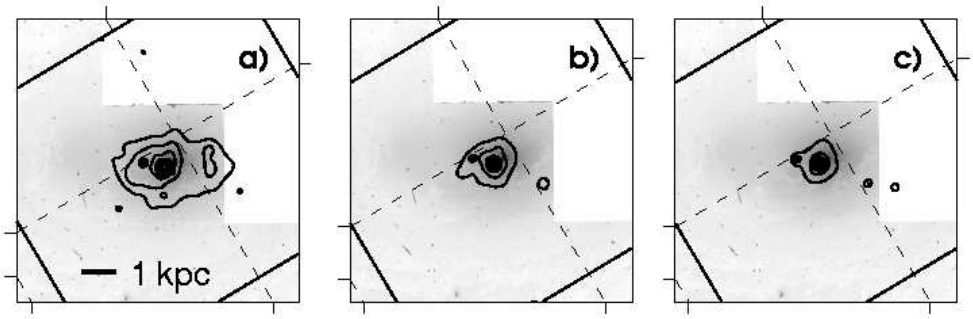

Figure 9. ACIS-S *contours* overlaid on an optical *HST* image of NGC 4579. Image size is $\sim 1.2' \times 1.2'$ ($\sim$ 10 kpc $\times$ 10 kpc). Energy bands are *a)* 0.2–1.5 keV, *b)* 1.5–2.5 keV and *c)* 2.5–8.5 keV.

its association with the radio emission implies shock heated gas along the radio lobe. The spectrum of the extended emission is well described as a 0.5–0.6 keV Mekal plasma with abundances < 0.14 times solar. Such temperatures indicate shock velocities of 660–690 km s^{-1}.

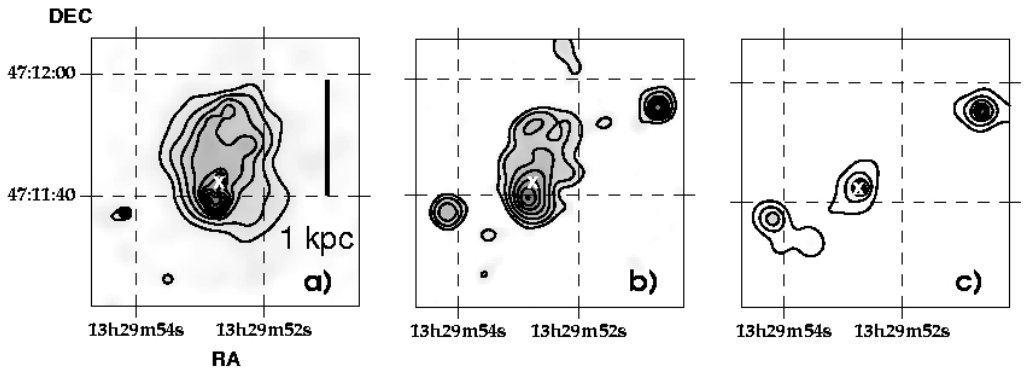

Figure 10. Adaptively smoothed *Chandra* images of M51 with *contours* overlaid for *a)* 0.2–1.5 keV, *b)* 1.5–2.5 keV and *c)* 2.5–8.5 keV. Image size is $1' \times 1'$(2.4 kpc $\times$ 2.4 kpc). *Crosses* mark the location of the galaxy nucleus for comparison between images.

The spectrum of the nucleus is dominated by reflection at hard energies. The best fitting model is a power law plus Fe K line plus Mekal plasma with $k\Gamma = 0.6$ keV. However, the plasma model prefers low abundances, similar to NGC 1068 (§3.1) and the X-ray jet in NGC 2110 (§3.2). For a power-law model, $N_{\rm H} = 3 \times 10^{23}$ cm^{-2}. *BeppoSAX* finds an additional heavily absorbed component with intrinsic $N_{\rm H} \sim 1 \times 10^{24}$ and an intrinsic X-ray luminosity of 2×10^{41} erg s^{-1} (Fukazawa et al. 2001).

4. Starbursts and Starburst-Powered X-rays

4.1. NGC 253

Figure 11 shows the adaptively smoothed, false-color *Chandra* images of the central $1.75' \times 2.0'$(1,365 pc × 1,560 pc) of NGC 253 in the soft, medium and hard X-ray bands defined as 0.2–1.5 keV, 1.5–4.5 keV and 4.5–8.0 keV, respectively. The medium and hards bands differ from those used for other galaxies discussed here and were chosen based on *ROSAT* and *ASCA* data to separate the various spectral components (Dahlem, Weaver & Heckman 1998). The true-color *Chandra* image is shown in Figure 12*a*. The central kpc harbors a collimated, limb brightened outflow. The coincidence of soft X-rays with Hα suggests that the X-rays in the nuclear plume are produced in the regions of interaction between the starburst and the dense ISM (Strickland et al. 2000).

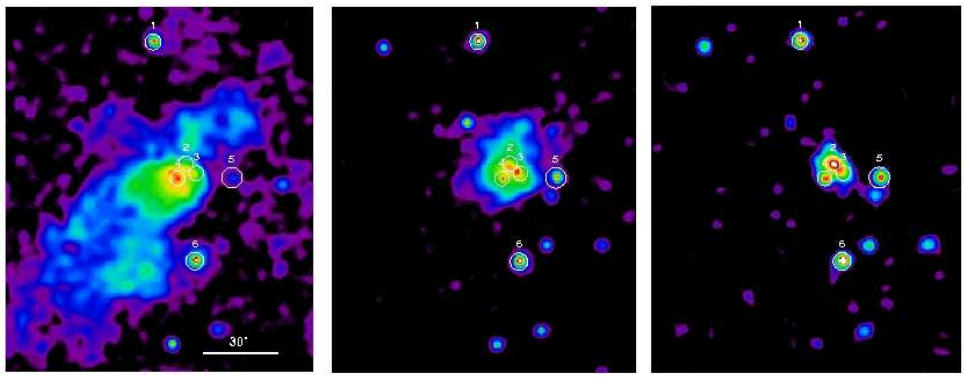

Figure 11. Soft, medium and hard-band adaptively smoothed (false-color) images of NGC 253. Image size is $1.1' \times 1.4'$. Ultraluminous X-ray point sources are numbered, including the core (#2).

The six brightest point sources within the central kpc are numbered in Figure 11. Source 2 is coincident with the galaxy nucleus, defined by the brightest compact radio source (Turner and Ho 1985). Regions of soft and hard X-ray emission have different morphologies. There is extended hard X-ray emission at the galaxy core associated with a ~ 100 pc ridge of molecular clouds defined by IR and radio observations. The numbered point sources all have luminosities at least 10 times larger than expected for the Eddington Limit of a ~ 1 $M_\odot$ accreting compact object.

The core has an unabsorbed $0.2 - 9$ keV flux of 6.7×10^{-13} erg cm^{-2} s^{-1}, $N_{\rm H} = 3 \times 10^{22}$ cm^{-2} and an unabsorbed luminosity of 2×10^{39} erg s^{-1}. It possesses a hard X-ray spectrum ($\Gamma \sim 1.3$) with copious line emission. A thermal model yields a temperature of 12 keV, which is consistent with what might be expected for hot gas in the starburst region (Chevalier & Clegg 1985); however, the emission lines are much stronger relative to the continuum than expected for a thermal plasma, suggesting that the continuum source is obscured from view. If the central source is buried and completely absorbed (requiring $N_{\rm H} \geq 10^{24}$), then the power-law continuum likely represents scattered X-rays

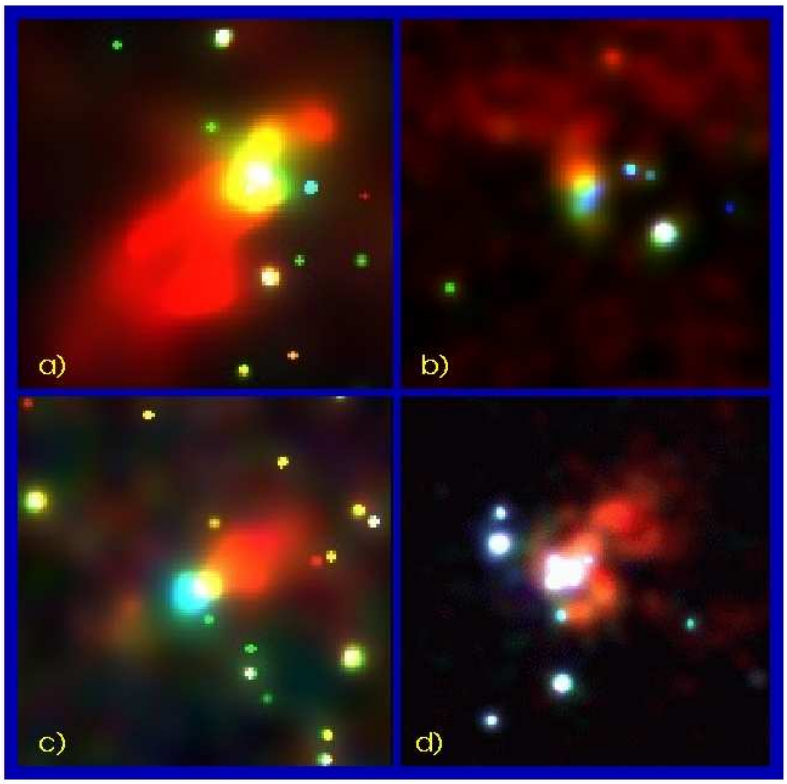

Figure 12. Adaptively smoothed "true-color" images of *a)* the central 0.9 kpc × 0.9 kpc region of NGC 253, *b)* the central 4 kpc × 4 kpc region of NGC 3628, *c)* the central 2.5 kpc × 2.5 kpc region of NGC 4945 and *d)* the central 1.6 kpc × 1.6 kpc region of Circinus. For NGC 3628, red is 0.3–1.0 keV, green 1–2 keV, blue 2–8 keV. For the other galaxies, red is 0.2–1.5 keV, green 1.5–2.5 keV, blue 2.5–8.5 keV.

from the central source reflected from the molecular clouds. In this case, the intrinsic nuclear luminosity is probably close to 1×10^{41} erg s^{-1}.

4.2. M 82

Chandra images of M 82 are shown in Figure 13. Within the central kpc, at least 11 distinct point sources are seen, some with significant variability (Matsumoto et al. 2001). However, unlike NGC 253, there is no compact X-ray source located at the center of the galaxy (Kaaret et al. 2001). The most luminous point source lies $9''(\sim 170$ pc) from the kinematic center of the galaxy (Matsumoto et al. 2001). Its variability places an upper limit on its size of 0.08 pc (Kaaret et al. 2001) and its luminosity ranges from about 10^{40} to 10^{41} erg s^{-1}, which corresponds to the Eddington luminosity for a 500 to 900 $M_\odot$ object.

The central kpc region is filled with diffuse hot gas, extending ~ 800 pc in the 2–8 keV band (Griffiths et al. 2000 and Fig. 13*c*). The diffuse emission makes

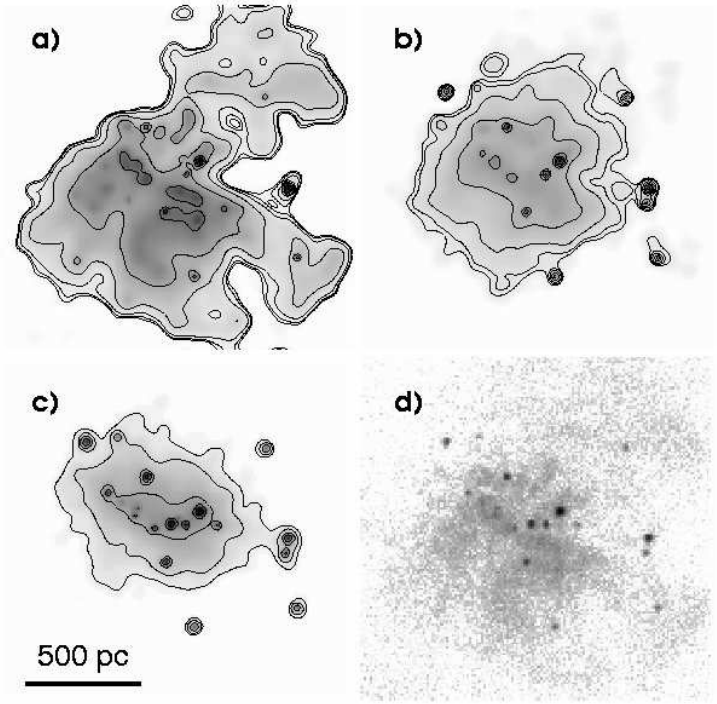

Figure 13. *a–c)* Adaptively smoothed *Chandra* ACIS-S greyscale images of the central $1.25' \times 1.25'$ (1.4 kpc $\times$ 1.4 kpc) region of M82 with *contours* overlaid. Energy bands are *a)* 0.2–1.5 keV , *b)* 1.5–2.5 keV and *c)* 2.5–8.5 keV. *d)* Unsmoothed ($0.5'' \times 0.5''$ pixels) full-band image (0.2–8.5 keV).

up about 30% of the total hard X-ray emission in the galaxy core and is at least partly thermal in origin, depending on assumptions about the physical state of the gas. M 82 has an unusually high temperature plasma core ($T \sim 4 \times 10^7$ K).

4.3. NGC 3628

The true-color, smoothed *Chandra* image of NGC 3628 is shown in Figure 12*b*. The blue dot at the center of the image represents the galaxy nucleus. The soft X-ray emission to the north is located on the top of the disk while there is strong absorption to the south.

The white circle is a well-known, variable ULX (or IXO) with an X-ray luminosity of $\sim 1 \times 10^{40}$ erg s^{-1}. It is located 900 ± 25 pc from the nucleus in projection (Strickland et al. 2001).

5. Starburst/AGN Composite Galaxies

5.1. NGC 3256

NGC 3256 is a merger-induced starburst system (Moran, Lehnert & Helfand 1999) with an X-ray luminous starburst having a luminosity of 1.6×10^{42} erg s^{-1}. *ASCA* data indicate that the soft X-rays are primarily thermal in origin, with $kT = 0.3$ and 0.8 keV, while the hard X-rays are best described as a power law. It has been suggested that NGC 3256 harbors two nuclei, one being a buried AGN

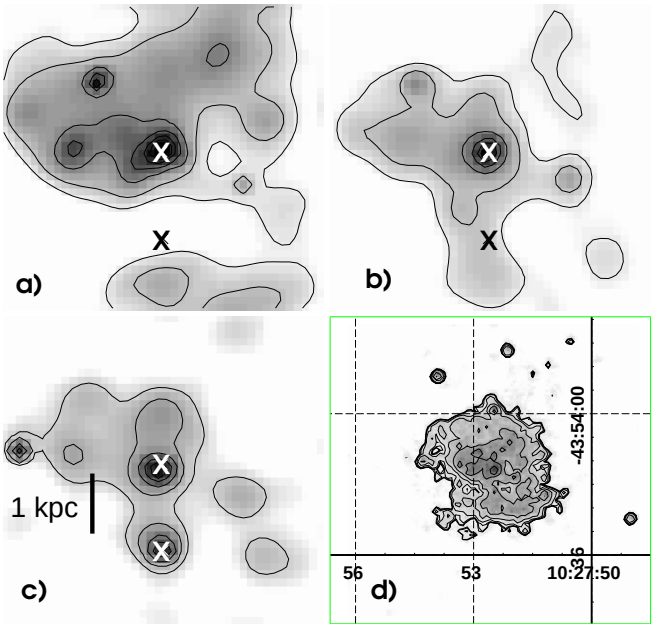

Figure 14. Grey-scale ACIS-S images of NGC 3256 with *contours* overlaid. The first three panels are $20'' \times 20''$ (5.4 kpc × 5.4 kpc) and represent the following energy bands: *a)* 0.2–1.5 keV *b)*, 1.5–2.5 keV and *c)* and 2.5–8.5 keV. The *lowest contours* are drawn approximately at the level of the local background. *d)* Adaptively smoothed full-band (0.2–8.5 keV) image with *contours* overlaid.

The *Chandra* image (Fig. 14) shows diffuse emission extended throughout the disk of the galaxy. At soft energies there is a single nuclear source, but at hard energies, two nuclei are clearly visible. The crosses mark the position of the optical nucleus (which has an IR and radio counterpart) and an IR and radio point source that is offset from the optical nucleus by about 1 kpc (Kotilainen et al. 1996). The two IR and radio nuclei are of comparable strength. The Chandra image shows that this is true in hard X-rays as well, confirming the possibility of a buried AGN with $N_{\rm H} \sim 10^{23}$ cm^{-2}.

5.2. NGC 4945

NGC 4945 shows a soft X-ray "plume" that lies perpendicular to the galaxy disk and extends $\sim$ 1 kpc from the nucleus (Fig. 15 and Fig. 12*c*). Like NGC 253,

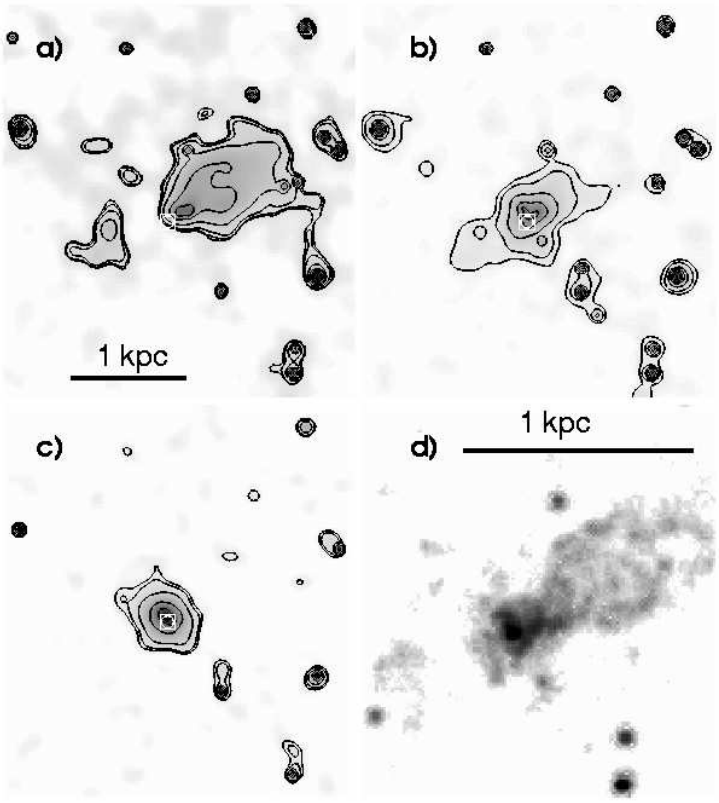

Figure 15. Adaptively smoothed *Chandra* ACIS images of NGC 4945 with *contours* overlaid. The first three panels are $1.0' \times 1.2'$(3.2 kpc × 3.8 kpc); the fourth is $30'' \times 36''$. Images are shown for energy bands *a)* 0.2–1.5 keV, *b)* 1.5–2.5 keV, *c)* 2.5–8.5 keV and *d)* 0.2–8.5 keV (total). The *white circle-in-square point* marks the position of the hard X-ray continuum peak for cross comparison of the images.

the soft X-rays suffer heavy absorption from the galaxy disk. The hard X-ray contours are slightly elongated in the direction of the galaxy disk which suggests some contribution from the starburst. The spectrum of the plume is dominated by soft X-ray lines from a combination of photoionized and collisionally ionized plasma. The nuclear spectrum is dominated by the Fe K line which presumably comes from a small (< 100 pc) region (G. M. Madejski, private communication).

5.3. Circinus

The soft X-ray emission from Circinus has an asymmetrical extension to the northwest in the direction of the optical ionization cone. The soft X-ray "plume" (Fig. 16 and Fig. 12*d*) coincides with the large-scale [O III] emission (Smith & Wilson 2001). The X-rays may be associated with a hot radiatively driven wind, shocks, or highly excited photoionized gas. Closer to the core on smaller scales

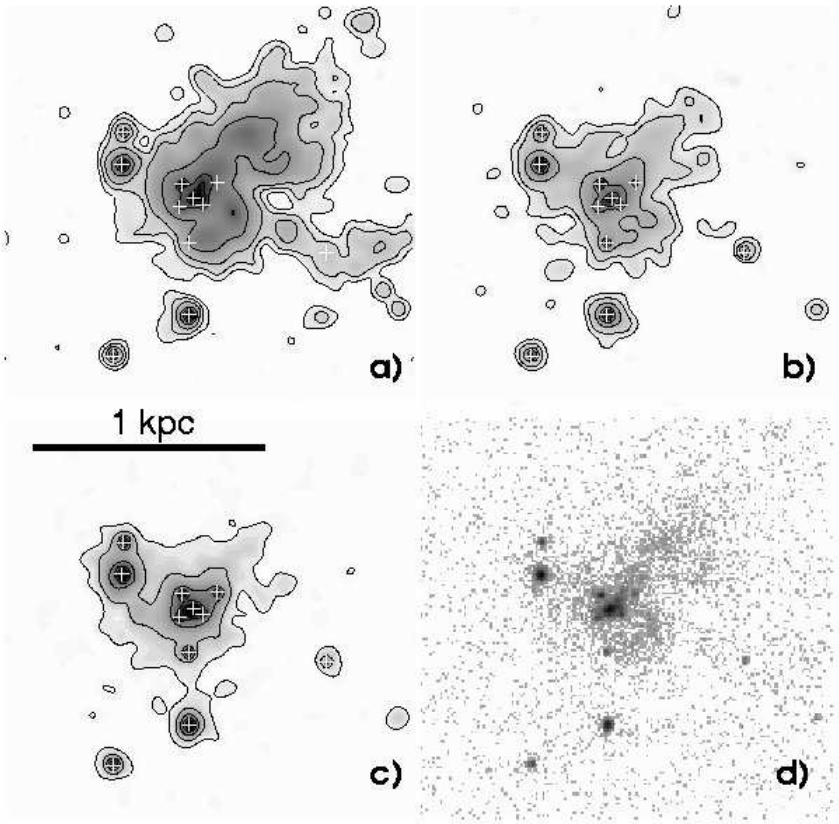

Figure 16. *a–c)* Adaptively smoothed ACIS-S images with *contours* for the central $1.4' \times 1.4'$ (1.6 kpc × 1.6 kpc) region of Circinus. Energy bands are *a)* 0.2–1.5 keV, *b)* 1.5–2.5 keV and *c)* 2.5–8.5 keV. *Crosses* mark the positions of the point sources. *d)* Unbinned and unsmoothed full-band image (0.2–8.5 keV).

($\sim$ 50 pc), soft X-rays are consistent with scattered nuclear radiation by ionized gas (Sambruna et al. 2001). The line emission is a a combination of highly ionized material together with a low-ionization reflector.

Eleven point sources are embedded in the diffuse X-ray emission. Bauer et al. (2001) report that few have optical counterparts within $1''$of their X-ray positions down to limiting magnitudes of m_V=23–25. The brightest is identified with the galaxy nucleus. At the distance of Circinus, their intrinsic 0.5–10 keV luminosities range from $\sim 2 \times 10^{37}$ to $\sim 4 \times 10^{39}$ erg s^{-1} with seven having L_X in excess of 1.3×10^{38} erg s^{-1}. One-fourth of the point sources vary and their spectral properties suggest that most are either black hole binaries or ultraluminous supernova remnants.

The ACIS spectrum of the nucleus exhibits emission lines at both soft and hard X-rays, including a prominent (EW $\sim$ 2.5) Fe Kα line at 6.4 keV. Fe Kα emission extends up to 200 pc from the nucleus (Smith & Wilson 2001).

6. Results Summary

Table 2 summarizes the spectral/spatial results from *Chandra* observations. For cases where results are not available in the literature (or current calibration issues preclude deriving them), results from other X-ray experiments such as *ASCA* and *BeppoSAX* are listed in italics.

Table 2. X-ray Spatial and Spectral Results

Galaxy	Nuclear Extent	# pt. src(1) within 1 kpc	Nuclear(2) Spectrum	$N_{\rm H}$ (10^{22})	Ref.(3)
NGC 253	$\sim$ 1 kpc	7	M,P,c	3	1
NGC 1068	550 pc	4	P,M,R,F,p,c	0.1,*1000*	2,3,*4*
NGC 2110	$\sim$ 1 kpc	0	P,M,F	3	
MCG$-$5-23-16	$<$ 1 kpc	–	P,F	5	
M 82	1 kpc	11	M,F,c	$\sim$ 1	5,6,7
NGC 3079	1.1 kpc	1	*M,P*	*1*	*8*
NGC 3256	–	2	*M,P*	*0.8*, 20	*9*
NGC 3628	$\sim$ 1 kpc	3	*M,P*	*0.9*	10, *8*
NGC 4051	$<$ 400 pc	1	P,F,p	0.1	11
NGC 4151	$\sim$ 1.5 kpc	1	P,F,p,c	3	12,13
NGC 4258	–	2	P,F	$\sim$ 1,*10*	14,*15*
NGC 4579	–	2	–	–	
NGC 4945	$\sim$ 1 kpc	4	P,F,p,c	*400*	*16*
M 51	800 pc	1	R,M,F,c	3, *600*	17, *18*
Circinus	60,600 pc	10	R,M,F,p,c	0.4,*400*	19,20,21,*4*

Notes.—(1) The number of X-ray point sources within 1 kpc of the nucleus, excluding the nucleus itself.

(2) Dominant continuum spectral components. P=power law, M=Mekal plasma, R=Compton reflection. Whether emission lines appear to be produced primarily from p=photoionization or c=collisional ionization. F indicates that an Fe K line is present.

(3) References: 1) Strickland, et al. 2000, 2) Young, et al. 2001, 3) Ogle 2001, 4) Bianchi, et al. 2001, 5) Griffiths, et al. 2000, 6) Matsumoto, et al. 2001, 7) Kaaret, et al. 2001, 8) Dahlem, et al. 1998, 9) Moran, et al. 1999, 10) Strickland, et al. 2001, 11) Collinge, et al. 2001, 12) Ogle, et al. 2000, 13) Yang, et al. 2001, 14) Wilson, et al. 2001, 15) Fiore, et al. 2001., 16) Madejski, et al. 2000, 17) Terashima & Wilson 2001, 18) Fukazawa, et al. 2001, 19) Sambruna, et al. 2001, 20) Bauer, et al. 2001, 21) Smith & Wilson 2001.

6.1. Extended Emission

All of the galaxies mentioned in this review, with the exception of NGC 4051 and MCG$-$5-23-16, possess extended soft X-ray emission. At least three galaxies,

namely NGC 1068, M 82 and Circinus, have significant extended hard X-ray emission. Ten of the 15 galaxies possess a distinct nuclear component of extended soft X-rays that resembles an outflow. The morphology of this nuclear extended emission falls into two categories, "plume-like" structures and linear "jet-like" structures.

Galaxies with X-ray plumes all possess starbursts. These are NGC 253, NGC 4945, NGC 3079, NGC 3628 and Circinus. M 82 is also plume-like although the nuclear emission is not as easily distinguished from the larger scale X-ray emission. The plumes range in size from ~ 600 pc to ~ 1 kpc and their spectra tend to be dominated by thermal emission.

Galaxies with X-ray jets are NGC 1068, NGC 2110, and NGC 4151. The X-ray features align with optical and radio counterparts and their sizes range from ~ 500 pc to ~ 1.5 kpc. The X-ray jets tend to have fairly featureless spectra; their spectra are not well described as thermal emission. The nuclei of galaxies with X-ray jets all harbor AGN and their nuclear spectra tend to be dominated by photoionization.

M 51 is unique in that its X-ray outflow resembles a cross between a jet and a plume. The X-rays have a radio counterpart, but the X-ray spectrum is thermal. This is perhaps the best case for shock heating resulting from an AGN-driven outflow.

The presence of an X-ray plume appears to depend on the presence of a starburst. Two of the most spectacular plumes occur in NGC 253, a starburst, and NGC 4945, a starburst with an AGN. It would appear that the collimating mechanisms are the same in these two nuclei. While it is fairly clear that the plume in NGC 253 is a superwind, in NGC 4945 it is not clear whether the outflow represents a superwind or an ionization cone. By analogy with NGC 253, it seems likely that the starburst is driving the outflow in NGC 4945 and that, in this case, the outflow is also the ionization cone.

6.2. The X-ray Spectra

Complex absorption structures are common in AGN and starbursts. The starburst region can have large X-ray column densities of up to a few times 10^{22} cm^{-2}. This is similar to the column densities seen in X-ray bright Seyfert 2s like NGC 2110 and MCG−5-2-16. But there are also multiple regions or layers of absorption in many of these galaxies. Buried AGN are often hidden behind absorbing columns a factor of 10 to 100 times higher than those measured with *Chandra* (Table 2). Examples are M 51, NGC 4945, NGC 1068 and Circinus.

Ten galaxies show prominent Fe Kα lines. MCG−5-23-16 and NGC 4051 have lines that are dominated by a narrow and unresolved core that cannot arise from the inner regions of an accretion disk. Fe K emission also is extended on NLR scales in at least two cases (Circinus and NGC 1068). Clearly, non-disk contributions to the Fe Kα emission in Seyfert galaxies are common.

6.3. Other X-ray point Sources Within the Central kpc

The galaxies with the largest number of X-ray point sources within their central kpc (excluding the actual nucleus) are galaxies with starbursts like NGC 253, M 82 and Circinus. Pure AGN have the fewest (0 to 2), while the other galaxies tend to have 1 to 4. It is important to examine more nearby galaxies to rule out

a selection effect since the galaxies with the most point sources are closest to us and hence individual sources are easier to detect. However, in NGC 253 and Circinus, many of the point sources are very bright and ultraluminous and similar sources could have been detected in at least some of the other galaxies. This suggests that near-nuclear ultraluminous sources are more common in galaxies with circumnuclear starbursts.

7. The Starburst-AGN Connection

I believe that the results presented here support the idea of an intimate connection between starburst and AGN activity. *Chandra* images and spectra offer powerful evidence for the interplay between stellar and non-stellar activity in the centers of nearby galaxies. The starburst region can have large X-ray column densities of up to a few times 10^{22} cm^{-2}. Such large absorption can obscure the central AGN at optical wavelengths, making a Seyfert 1 galaxy in to a Seyfert 2 without requiring a pc-scale molecular torus. A similar effect has been inferred for a large *ASCA* sample of AGN with starbursts (Levenson, Weaver & Heckman 2001).

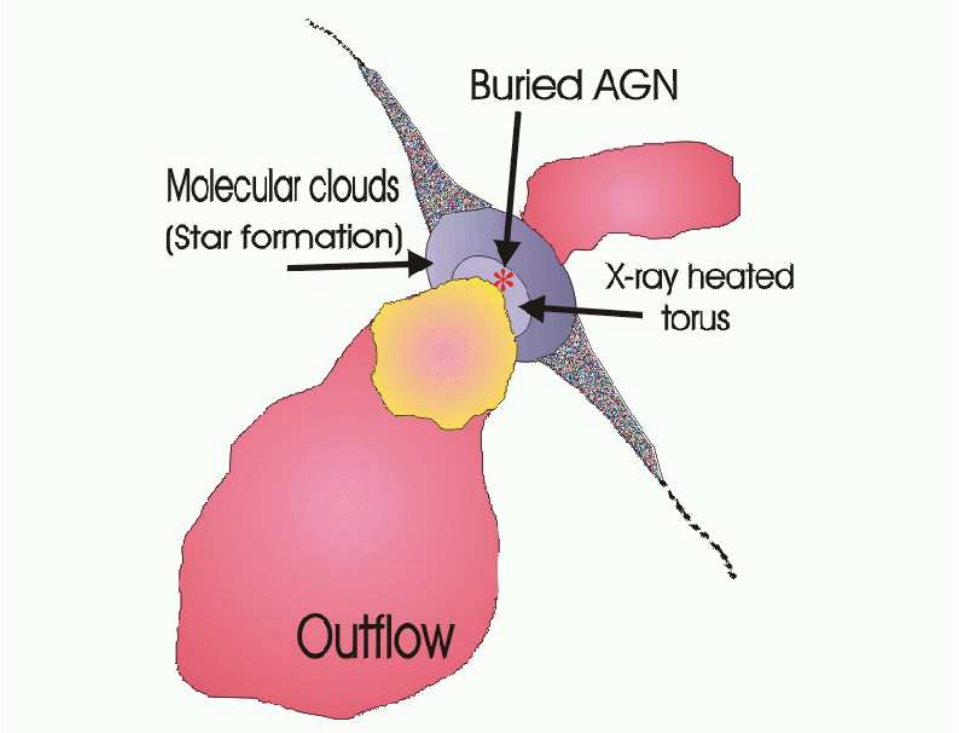

Figure 17. Cartoon of the central kpc of a starburst-AGN composite ("energetic") galaxy.

A physical model for the center of an energetic galaxy is proposed in Figure 17, which shows a cartoon of an AGN buried within a circumnuclear starburst. If active, the AGN will photoionize the inner edge of the ring of molecular clouds

associated with the starburst, creating a large-scale X-ray heated torus. The emergent nuclear spectrum would be complex, showing features of reflection, ionized absorption, photoionization, collisional excitation and fluorescence, similar to many of the *Chandra* spectra. This problem is similar to that of X-ray heated winds in AGN (Krolik & Kriss 1995) but adding a secondary source of ionization and/or heating from the starburst.

Figure 18 shows a revised version of the standard unified model for AGN. On the pc scale is the Compton-thick molecular torus, needed to provide the heavy obscuration of the central source in objects like NGC 1068, NGC 4945, M 51. At distances of ∼50–100 pc are the starburst region clouds with column densities of 10^{22-23} cm^{-2}, enough to obscure X-ray bright Seyfert 2s like NGC 2110, MCG−5-23-16 (a starburst "curtain"). Depending on the alignment of the Seyfert nucleus with the starburst geometry, the ionization cone could be blocked or even further collimated by the starburst.

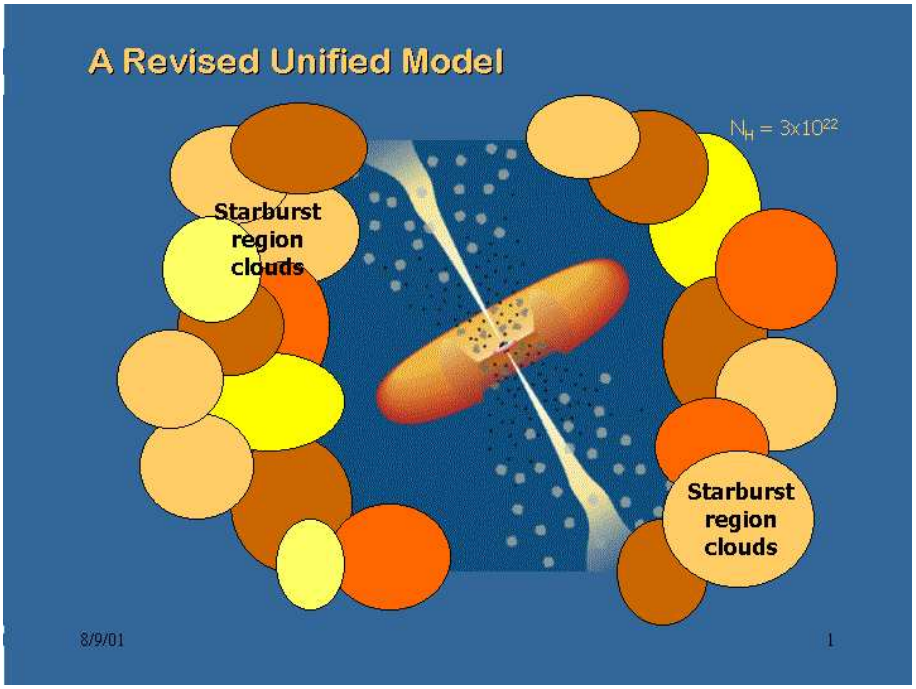

Figure 18. Cartoon of a revised unified model, which includes a central AGN surrounded by the standard pc-scale Compton-thick torus plus an obscuring region of ∼ 50 pc diameter of dense molecular clouds ($N_{\rm H} = 10^{22-23}$ cm^{-2}) associated with a circumnuclear starburst.

It has been proposed that circumnuclear starburst activity and nuclear activity could both be triggered by gas accreting toward the nucleus. This gas could also be responsible for obscuring the AGN in its early stages of formation (Sanders et al. 1988). Indeed, Oliva et al. (1999) find that old and powerful starbursts are common in obscured AGN. It has also been suggested that a starburst could evolve into an AGN by building up a massive star cluster at the center of a galaxy which then triggers an AGN by feeding a central black hole

as a result of mass loss (Norman & Scoville 1988). Galaxies may cycle through phases where the starburst outshines the AGN and vice versa.

Finally, bright off-nuclear X-ray point sources (some being ULXs with possible masses of 10–1,000 $M_{\odot}$) appear to be common in circumnuclear starburst regions. It is possible that such ULX black holes (if they are indeed intermediate mass black holes) may be the precursors to AGN activity. If born in dense star clusters near the centers of galaxies, ULX BHs could sink to the core via dynamical friction, eventually growing into a supermassive black hole (Tremaine, Ostriker & Spitzer 1975; Quinlan & Shapiro 1990).

Acknowledgments. Thanks to David Strickland, Patrick Ogle and Greg Madejski for communicating results prior to publication. This research has made use of the NASA/IPAC Extragalactic Database (NED) which is operated by the Jet Propulsion Laboratory, California Institute of Technology, under contract with the National Aeronautics and Space Administration. The Digitized Sky Survey was produced at the Space Telescope Science Institute under U.S. Government grant NAG W-2166. The images of these surveys are based on photographic data obtained using the Oschin Schmidt Telescope on Palomar Mountain and the UK Schmidt Telescope.

References

Baur, F. E., Brandt, W. N., Sambruna, R. M., Chartas, G., Garmire, G. P., Kaspi, S. & Netzer, H. 2001, AJ, 122, 182

Bianchi, S., Matt, G. & Iwasawa, K. 2001, MNRAS, 322, 669

Chevalier, R. A. & Clegg, A. W. 1985, Nature, 317, 44

Colbert, E. J. M. & Mushotsky, R. F. 1999, ApJ, 519, 89

Collinge, M. J. et al. ApJ in press (astro-ph/0104125)

Dahlem, M., Weaver, K. A. & Heckman, T. M. 1998, ApJS, 118, 401

Fiore, F., et al. 2001, ApJ, 556, 150

Fukazawa, Y., Iyomoto, N., Kubota, A., Matsumoto, Y. & Makishima, K. 2001, AA, 374, 73

Griffiths, R. E., Ptak, A., Feigelson, E. D., Garmire, G., Townsley, L., Brandt, W. N., Sambruna, R. & Bregman, J. N. 2000, Science, 290, 1325

Kaaret, P., Prestwich, A. H., Zezas, A., Murray, S. S., Kim, D.-W., Kilgard, R. E., Schlegel, E. M. & Ward, M. J. 2001, MNRAS, 321, L29

King, A. R., Davies, M. B., Ward, M. J., Fabbiano, G. & Elvis, M. 2001, ApJ, 552, 109

Kotilainen, J. K., Moorwood, A. F. M., Ward, M. J. & Forbes, D. A. 1996, AA, 305, 107

Krolik, J. H. & Kriss, G. A. 1995, ApJ, 447, 512

Levenson, N. A., Weaver, K. A. & Heckman, T. M. 2001, ApJ, 550, 230

Madejski, G., Zycki, P., Done, C., Valinia, A., Blanco, P., Rothschild, R. & Turek, B. 2000, ApJ, 535, L87

Makishima, K., et al. 2000, ApJ, 535, 632

Maiolino, R., Ruiz, M. Rieke, G. H. & Keller, L. D. 1995, ApJ, 446, 561

Matsumoto H., Tsuru, T. G., Koyama, K., Awaki, H., Canizares, C. R., Kawai, N., Matsushita, S. & Kawabe, R. 2001, ApJ, 547, L25

Moran, E. C., Lehnert, M. D. & Helfand, D. J. 1999, ApJ, 526, 649

Nandra, K., George, I. M., Mushotzky, R. F., Turner, T. J. & Yaqoob, T. 1997, ApJ, 476, 70

Norman, C. & Scoville, N. 1988, ApJ, 332, 124

Ogle, P. M. 2001, *Mass Outflow in AGN: New Perspectives*, ASP conference Series (eds. Crenshaw, Kraemer & George), in press

Ogle, P. M., Marshall, H. L., Lee, J. C. & Canizares, C. R. 2000, ApJ, 545, L81

Oliva, E., Origlia, L., Maiolino, R. & Moorwood, A. F. M. 1999, AA, 350, 9

Quinlan, G. D. & Shapiro, S. L. 1990, ApJ, 356, 483

Sambruna, R. M., Brandt, W. N., Chartas, G., Netzer, H., Kaspi, S., Garmire, G. P., Nousek, J. A. & Weaver, K. A. 2001, ApJ, 546, L9

Sanders, D. B., Soifer, B. T., Elias, J. H., Neugebauer, G. & Matthews, K. 1988, ApJ, 328, L35

Smith, D. A. & Wilson, A. S., ApJ in press (astro-ph/0104252)

Strickland, D. K., Heckman, T. M., Weaver, K. A. & Dahlem, M. 2000, AJ, 120, 2965

Strickland, D. K., Colbert, E. J. M., Heckman, T. M., Weaver, K. A., Dahlem, M. & Stevens, I. R., ApJ in press (astro-ph/0107115)

Terashima, Y. & Wilson, A. S. ApJ in press (astro-ph/0103287)

Tremaine, S. D., Ostriker, J. P. & Spitzer, L., Jr. 1975, ApJ, 196, 407

Turner, J. L. & Ho, P. T. P. 1985, ApJ, 299, L77

Ulvestad, J. S. & Wilson, A. S. 1983, ApJ, 264, L7

Veilleux, S., Cecil, G., Bland-Hawthorn, J., Tully, R. B., Filippenko, A. V. & Sargent, W. L. W. 1994, ApJ, 433, 48

Weaver, K. A., Yaqoob, T., Mushotzky, R. F., Nousek, J., Hayashi, I. & Koyama, K. 1997, ApJ, 474, 675

Wilson, A. S. & Ulvestad, J. S. 1983, ApJ, 275, 8

Wilson, A. S., Yang, Y., & Cecil, G. ApJ in press (astro-ph/0106514)

Yang, Y., Wilson, A. S. & Ferruit, P. ApJ in press (astro-ph/0108166)

Young, A. J., Wilson A. S. & Shopbell, P. L. 2001, ApJ, 556, 6